Journal of Volcanology and Geothermal Research 387 (2019) 106658

Contents lists available at ScienceDirect

Journal of Volcanology and Geothermal Research

journal homepage: www.elsevier.com/locate/jvolgeores

Conduit dynamics of highly explosive basaltic eruptions: The 1085 CE Sunset Crater sub-Plinian events

G. La Spina [a,*], A.B. Clarke [b,c], M. de' Michieli Vitturi [c], M. Burton [a], C.M. Allison [b], K. Roggensack [b], F. Alfano [b]

[a] School of Earth and Environmental Sciences, The University of Manchester, UK
[b] School of Earth and Space Exploration, Arizona State University, Tempe, AZ, USA
[c] Istituto Nazionale di Geofisica e Vulcanologia, Sezione di Pisa, Italy

ARTICLE INFO

Article history:
Received 13 March 2019
Received in revised form 29 July 2019
Accepted 3 August 2019
Available online 7 August 2019

Keywords:
Magma ascent
Conduit model
Basalt
Explosive eruption
Magma chamber
Sunset Crater

ABSTRACT

Basaltic volcanoes produce a range of eruptive styles, from Strombolian to low-intensity fire fountaining to, much more rarely, highly explosive Plinian eruptions. Although the hazards posed by highly explosive eruptions are considerable, controlling mechanisms remain unclear, and thus improving our understanding of such mechanisms is an important research objective. To elucidate these mechanisms, we investigate the magma ascent dynamics of basaltic systems using a 1D numerical conduit model. We find that variations in magmatic pressure at depth play a key role in controlling modelled eruption characteristics. Our most significant result is that a decrease in pressure at depth, consistent with the emptying of a magma chamber, results in enhanced volatile exsolution and in deepening fragmentation depth. The corresponding decrease in conduit pressure ultimately produces a collapse of the conduit walls. This type of collapse may be a key mechanism responsible for the cessation of individual explosive eruptions, a notion previously explored for silicic eruptions, but never before for basaltic systems. Using previously published field and sample analysis to constrain model parameters, we simulate scenarios consistent with sub-Plinian eruptions, similar to those at Sunset Crater volcano in ~1085 CE in terms of mass eruption rates and duration. By combining these analyses with a chamber-emptying model, we constrain the size of the magma chamber at Sunset Crater to be on the order of tens of km^3. During the 1085 CE Sunset Crater eruption, there were three main sub-Plinian events that erupted between 0.12 and 0.33 km^3 of tephra (non-DRE), indicating that ~1% of the total chamber volume was erupted during each sub-Plinian pulse.

1. Introduction

Among the different eruptive activities that a volcano can exhibit, explosive eruptions are the most intense and violent. These eruptions can inject very large volumes of a gas-particle mixture into the atmosphere over different timescales (seconds to weeks), generating columns that may reach up to tens of kilometres in height. Several styles of explosive eruptions exist: Hawaiian, Strombolian, Vulcanian, violent Strombolian, sub-Plinian and Plinian eruptions. Typical Hawaiian eruptions are characterized by fire-fountaining activities sustained for hours to weeks (Richter et al., 1970; Gonnermann and Manga, 2013), which can reach heights of several hundred meters. Strombolian eruptions consist of periodic impulsive explosions caused by the bursting of an overpressured gas slug at the surface (Walker, 1973; Houghton and Gonnermann, 2008; Gonnermann and Manga, 2013). Vulcanian eruptions are characterized by short-lived (typically seconds to minutes), discrete explosions caused by sudden decompression of a volcanic conduit (Mercalli, 1907; Clarke, 2013; Clarke et al., 2015; La Spina et al., 2017a). In contrast, Plinian eruptions are quasi-steady explosive eruptions, sustained for hours to days, generating buoyant vertical columns up to 30 km high (Costantini et al., 2010; Gonnermann and Manga, 2013; Cioni et al., 2015). The characteristics of sub-Plinian and violent Strombolian eruptions are similar to those of Plinian eruptions, but have lower mass eruption rates and lower eruptive columns, ranging between 10 and 20 km in altitude (Bursik, 1993; Cioni et al., 2003, 2015) and up to 10 km (Valentine, 1998; Valentine and Gregg, 2008; Pioli et al., 2008), respectively.

Vulcanian, sub-Plinian, or Plinian explosive activity is favored in high viscosity silicic magmas, whereas Hawaiian or Strombolian activity is common in basaltic systems. Occasionally, however, basaltic volcanoes produce highly explosive eruptions, up to Plinian in scale with mass discharge rates of ~10^8 kg/s (Williams, 1983; Walker et al., 1984; McPhie et al., 1990; Coltelli et al., 1998; Nye et al., 2002; Rosi et al., 2006; Scollo et al., 2007; Houghton and Gonnermann, 2008; Costantini et al., 2010; Schauroth et al., 2016). While Mt. Etna (Italy), for example, has generated multiple Strombolian, fire-fountaining and sub-Plinian events during the last 20 years (Branca and Del Carlo, 2005; Polacci

* Corresponding author.
E-mail address: giuseppe.laspina@manchester.ac.uk (G. La Spina).

https://doi.org/10.1016/j.jvolgeores.2019.08.001

et al., 2006; Behncke et al., 2014; Pompilio et al., 2017), it also has produced historical highly explosive eruptions, such as the Plinian event that occurred in 122 BCE (Coltelli et al., 1998; Giordano and Dingwell, 2003; Pompilio et al., 2017). This type of unexpected eruption poses a real challenge to policy-makers when mitigating the risks associated with basaltic volcanoes. Therefore, a clearer understanding of the processes controlling the ascent of basaltic magma and corresponding eruption styles is of paramount importance.

During magma ascent several interdependent processes take place, such as gas exsolution and expansion, outgassing, crystallization, temperature change, and associated rheological variations. Although laboratory experiments, field work, thermodynamic modelling, and analytical measurements provide essential data to understand each of these processes (such as Costantini et al., 2009; Costantini et al., 2010; Agostini et al., 2013, Arzilli et al., 2015, Di Genova et al., 2017, Petrelli et al., 2018, Polacci et al., 2018, Moitra et al., 2018, Alfano et al., 2018 and Allison et al., 2019), the highly non-linear interdependence of magma ascent processes makes the understanding of overall ascent behaviour challenging to unravel. From this perspective, numerical models of magma ascent, which are able to couple and integrate all of these processes at the same time, constrained by field observations of eruptions and analysis of eruptive products, provide an invaluable tool for investigating eruption dynamics of basaltic volcanoes (La Spina et al., 2015, 2016, 2017b).

Over the course of the past decades, numerical models of magma ascent dynamics have been widely used to investigate highly explosive silicic eruptions (Wilson et al., 1980; Dobran, 1992; Papale and Dobran, 1994; Papale, 1999; Melnik, 2000; Papale, 2001; Gonnermann and Manga, 2003; Costa et al., 2009a, 2009b; Kozono and Koyaguchi, 2009; Degruyter et al., 2012; La Spina et al., 2017a; Aravena et al., 2017, 2018a, 2018b). On the other hand, there exist only a few studies of magma ascent dynamics in basaltic eruptions, mainly focused on effusive, Strombolian, and fire-fountaining activities (Wilson and Head, 1981; Vergniolle and Jaupart, 1986; Parfitt, 2004; Rutherford and Papale, 2009; La Spina et al., 2015, 2016, 2017b). Mechanisms controlling highly-explosive basaltic eruptions thus remain unclear.

Here we investigate the magma ascent dynamics of basaltic sub-Plinian to Plinian eruptions by adopting a 1D numerical conduit model for magma ascent and varying key input parameters over a range of values to discover general trends and thresholds. We focus our attention on the 1085 CE basaltic sub-Plinian eruptions at Sunset Crater volcano, Flagstaff, AZ, USA (Fig. 1), and by extension also on systems with similar magma characteristics. Using several types of previously published field observations, we constrain input parameters for the Sunset Crater conduit model, including pressure at depth, temperature, and volatile and crystal contents. We then analyse how varying input parameters affects key output variables, including mass eruption rate and exit velocity. Finally, we study what controls eruption duration and provide some insights into magma storage at depth.

2. Materials and methods

2.1. The steady conduit model

In this work we use the 1D steady-state model for magma ascent in a cylindrical conduit described by La Spina et al. (2015, 2016, 2017b). In general, however, volcanic plumbing systems are more complicated than a simple cylindrical conduit geometry. For this reason, a discussion on the assumption of the cylindrical conduit geometry for our test case study will be presented in Section 3. The executable for Windows, Linux and macOS of this version of the conduit model can be downloaded from the link bit.ly/MAMMA_CODE_v0d2. The system of differential equations is derived from the theory of thermodynamically compatible systems (Romenski et al., 2010), where conservation equations for the mixture are coupled with equations describing disequilibrium between phases. A schematic representation of magma ascent dynamics during explosive eruptions in a conduit-like geometry is illustrated in Fig. 2.

Fig. 1. Sunset Crater volcano, photo taken from SW.

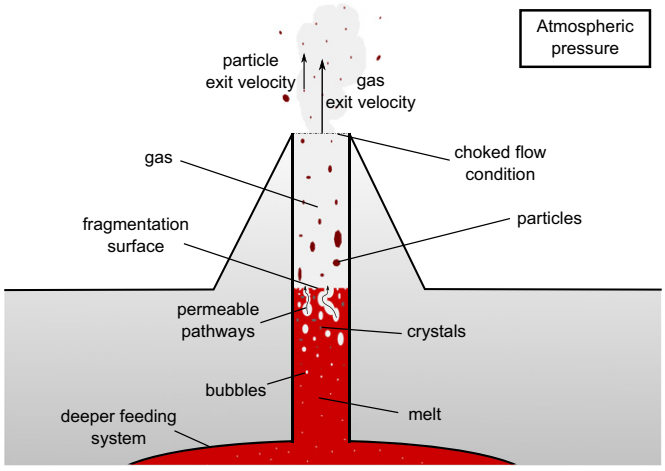

Fig. 2. Schematic picture of magma ascent dynamics during explosive eruptions in a conduit-like geometry.

In this model, the magmatic mixture is assumed to be a combination of two phases. Below the fragmentation level, the mixture is composed of a liquid phase (denoted by the index l), made of a mixture of melt, crystals and dissolved volatiles, and a gas phase (denoted by the index g), consisting of bubbles of exsolved volatiles. Above the fragmentation level, the liquid phase is replaced by a dispersed particle phase (still denoted by index l), whereas the gas phase continues to represent the mixture of exsolved volatiles. Since the gas mixture is always referred to as the exsolved volatile phase, we can use, without ambiguity, the subscripts g_1 and g_2 to refer to the two main gas species present in a magmatic mixture: H_2O and CO_2. The subscripts d_1 and d_2, instead, are used to refer to the dissolved volatile species, whereas the subscript m is used for the melt, and c for the total crystal content. Each of the two phases of the mixture and each component is characterized by the volume fraction (α_k), mass density (ρ_k), mass fraction (x_k), velocity (u_k), specific internal energy (e_k), specific entropy (s_k), pressure (P_k) and temperature (T_k). Therefore, the saturation constraints of $\alpha_l + \alpha_g = 1$ and $x_l + x_g = 1$ hold all along the conduit. Within each phase, we assume that all components have the same pressure, temperature and velocity (i.e. $P_m = P_c = P_{d_i} = P_l$ and $P_{g_i} = P_g$, and analogously for the temperature and velocity). Using the notation described above, we define the mixture parameters as follows:

$$\begin{aligned} &\rho = \alpha_l\rho_l + \alpha_g\rho_g; \quad && P = \alpha_l P_l + \alpha_g P_g; \\ &x_l = \frac{\alpha_l\rho_l}{\rho}; && T = \alpha_l T_l + \alpha_g T_g; \\ & && u = x_l u_l + x_g u_g; \\ & && e = x_l e_l + x_g e_g; \\ &x_g = \frac{\alpha_g\rho_g}{\rho}; && s = x_l s_l + x_g s_g. \end{aligned} \tag{1}$$

Relative motion between gas and liquid/particle phase is permitted, and different pressures between the gas and the liquid/particle phase can also be considered. An equilibrium temperature is assumed between the two phases. La Spina et al. (2015) have shown that temperature profile varies along the conduit, mainly due to adiabatic gas expansion, resulting in a cooling of the magmatic mixture, and crystallization, which produces a heating of the system. Furthermore, other processes, such as heat loss to wall rocks and viscous heating due to friction with conduit walls, may occur during magma ascent causing temperature variations within the conduit (Costa et al., 2007; Lavallée et al., 2015). Due to the strong coupling between temperature and viscosity (Costa et al., 2007; Giordano, 2019), these variations can potentially affect magma ascent dynamics. However, since in this work we are modelling just the last few hundred meters below the vent, we can infer that the temperature variations within the shallow part of the conduit are minimal (Campagnola et al., 2016). Moreover, we do not have tight constraints on the temperature at the inlet to the shallow conduit. For these reasons, as done previously by several authors (such as Melnik and Sparks, 2002; Macedonio et al., 2005; Kozono and Koyaguchi, 2009; Rutherford and Papale, 2009; Degruyter et al., 2012; Moitra et al., 2018), we adopted, as a first order approximation, isothermal conditions ($T_l = T_g = T \equiv constant$), and then investigate different inlet temperatures via sensitivity analysis.

Following La Spina et al. (2015, 2017b), the conservation equations for the mixture mass and momentum are:

$$\frac{\partial \rho u}{\partial z} = 0, \tag{2}$$

$$\frac{\partial}{\partial z}\left[\sum_{k=l,g}\alpha_k\rho_k u_k^2 + \alpha_k P_k\right] = -\rho g - f_{D_l}\frac{\rho_l u_l^2}{4r}\left(1-\phi_f\right) - f_{D_g}\frac{\rho_g u_g^2}{4r}\phi_f. \tag{3}$$

Here, g is gravitational acceleration, ϕ_f is a non-dimensional variable, which is 0 below the fragmentation level and 1 otherwise, r is the conduit radius, which is assumed to be constant, and f_{D_l} and f_{D_g} are the Darcy-Weisbach friction factors, which are functions of Reynolds number (and therefore of viscosity) and conduit wall roughness as per the empirically-derived Moody diagram (Weisbach, 1845; Brown, 2003).

The following balance equation defines variations in the liquid volume fraction, and thus also in the gas volume fraction, along the conduit:

$$\frac{\partial \rho u \alpha_l}{\partial z} = -\frac{1}{\tau^{(p)}}\left(P_g - P_l\right). \tag{4}$$

The relaxation parameter $\tau^{(p)}$ ($m^2\ s^{-1}$) defines the disequilibrium between the gas and liquid pressures (La Spina et al., 2015). Here we assume equilibrium between the two pressures by setting $\tau^{(p)} \ll 1$.

The exsolution of each gas component and the corresponding dissolved contents are governed by the following balance equations:

$$\frac{\partial \alpha_{g_i}\rho_{g_i}u_g}{\partial z} = -\frac{1}{\tau^{(e)}}\left(x_{d_i}^{md} - x_{d_i}^{md,eq}\right)\left(\alpha_l\rho_l - \alpha_l\rho_c\beta_c\right), \tag{5}$$

$$\frac{\partial}{\partial z}\left(\left(\alpha_l\rho_l - \alpha_l\rho_c\beta_c\right)x_{d_i}^{md}u_l\right) = \frac{1}{\tau^{(e)}}\left(x_{d_i}^{md} - x_{d_i}^{md,eq}\right)\left(\alpha_l\rho_l - \alpha_l\rho_c\beta_c\right), \tag{6}$$

where $x_{d_i}^{md}$ is the mass fraction of the dissolved gas phase i with respect to the liquid crystal–free phase, while $x_{d_i}^{md,\,eq}$ is the value at equilibrium. The relaxation parameter $\tau^{(e)}$ (s) controls the exsolution rate and thus controls how close the dissolved gas mass fraction is to the equilibrium value. In this work we obtain instantaneous relaxation to the equilibrium value by setting $\tau^{(e)} \ll 1$.

Since we are interested in simulating sub-Plinian to Plinian eruptions of basaltic magma, we expect that the magma ascended rapidly all along the conduit, leaving insufficient time for crystallization during ascent and thus we assume a constant crystal content. This assumption for our case study will be discussed in Section 3.

Finally, the relative motion of the gas with respect to the liquid phase is expressed by the following differential equation:

$$\begin{aligned} &\frac{\partial}{\partial z}\left[\frac{u_l^2}{2} - \frac{u_g^2}{2} + e_l + \frac{P_l}{\rho_l} - e_g - \frac{P_g}{\rho_g} - (s_l - s_g)T\right] = \\ &-\frac{1}{\tau^{(f)}}\frac{\rho}{\rho_l\rho_g}\left(u_l - u_g\right) - f_{D_l}\frac{u_l^2}{4\alpha_l r}\left(1-\phi_f\right) + f_{D_g}\frac{u_g^2}{4\alpha_g r}\phi_f. \end{aligned} \tag{8}$$

The relaxation parameter $\tau^{(f)}$ ($kg^{-1}m^3s$) controls the degree of decoupling between the gas and the liquid phase. When this relaxation parameter is very small, the relative velocity approaches zero, whereas large values of $\tau^{(f)}$ result in strong decoupling. The model presented above is a general formulation, and can be used to describe magma

ascent dynamics for a wide range of volcanoes and eruptive regimes (La Spina et al., 2015, 2016). The application to a specific volcano is achieved by providing constitutive equations to describe the specific rheological, solubility, crystallization, outgassing, and fragmentation behaviour of the system, along with equations of state.

2.2. Constitutive equations and equations of state

In order to reproduce the magma ascent dynamics of highly-explosive basaltic eruptions, we selected constitutive equations that reasonably represent the Sunset Crater magmatic system, an alkali basalt similar in composition to that of Stromboli (Italy), Etna, and the Tecolote cone in the Pinacate Volcanic Field (Mexico). With respect to constitutive equations previously adopted by La Spina et al. (2015, 2016, 2017b) for Stromboli, Etna and Kilauea (HI, USA), we modify them to include the effects of bubbles on magma viscosity, refine the solubility models for water and carbon dioxide, and define friction at the conduit wall for both laminar and turbulent regimes. These new constitutive equations are described below. Regarding outgassing, following La Spina et al. (2017b), the relaxation parameter $\tau^{(f)}$ is defined by Forchheimer's law (Degruyter et al., 2012) below the fragmentation depth, while above the fragmentation level it is modelled according to Yoshida and Koyaguchi (1999). Fragmentation is assumed to occur at a critical gas volume fraction (Sparks, 1978) of 0.6, consistent with the vesicularity measured for Sunset scoria clasts (Alfano et al., 2014). Although the critical volume fraction criterion has been shown to be an oversimplification (Papale, 1999; Zhang, 1999), Melnik and Sparks (2002) and Degruyter et al. (2012) compare fragmentation criteria in one-dimensional conduit models, such as strain-rate, bubble overpressure, and bubble volume fraction, and demonstrate that different criteria lead to similar results in terms of eruption dynamics, largely because the thresholds are reached simultaneously. The equations of state adopted in this work are those described by La Spina et al. (2014, 2015).

2.2.1. Magma rheology

The viscosity of the liquid phase is modelled as:

$$\mu_l = \mu_{melt}\theta_c\theta_b, \tag{9}$$

where μ_{melt} is the viscosity of the bubble-free, crystal-free liquid phase, θ_c is a factor which increases viscosity due to the presence of crystals (Costa, 2005), and θ_b is a factor taking into account the effect of bubbles on the magmatic mixture. To estimate μ_{melt} as a function of melt composition, water concentration, and temperature we use the viscosity model of Giordano et al. (2008). In this work, we use the average composition of 1085 CE Sunset Crater scoria (Allison et al., 2019; Table 1). The presence of crystals is accounted for by θ_c as described in Costa et al. (2009a) and La Spina et al. (2015).

In a liquid mixture, the variation in viscosity due to the presence of bubbles depends on bubble response to shear stresses. Bubbles that remain spherical and undeformed serve to increase effective viscosity of the magma whereas those that deform easily serve to decrease effective viscosity (Llewellin et al., 2002; Llewellin and Manga, 2005; Mader et al., 2013). This bubble response can be described by the capillary number *Ca*, a dimensionless number representing the ratio between the viscous stress acting on the bubble and the restoring stress supplied by the surface tension (Mader et al., 2013):

$$Ca = \frac{\mu_{melt}\theta_c r_b \gamma_{shear}}{\Gamma}. \tag{10}$$

The capillary number depends on liquid viscosity (melt + crystals), shear strain rate (γ_{shear}), surface tension at the liquid-bubble interface (Γ), and bubble radius (r_b), which here is calculated as a function of the bubble number density (N_d) as reported in Degruyter et al. (2012). For this work we estimate N_d to be 10^{10} m^{-3} based on preliminary observations of scoria clasts from Sunset Crater, which are similar to values for the normal explosive activity at Stromboli (Polacci et al., 2009). Moreover, since our model is one-dimensional, the shear strain rate is computed as the mixture velocity divided by the conduit radius.

We adopt the general formulation for relative viscosity due to the presence of bubbles in a magmatic mixture presented by Llewellin et al. (2002). Following Mader et al. (2013), this equation can be generalized for non-dilute suspensions as

$$\theta_b = \theta_{b,\infty} + \frac{\theta_{b,0} - \theta_{b,\infty}}{1 + (K\,Ca)^m}, \tag{11}$$

$$\theta_{b,0} = (1-\alpha_g)^{-1}, \tag{12}$$

$$\theta_{b,\infty} = (1-\alpha_g)^{5/3}, \tag{13}$$

where $K = 6/5$ and $m = 2$.

2.2.2. Volatile solubility model

In this model, we consider two main gas components, water and carbon dioxide. The equilibrium dissolved water content as a function of water fugacity has been modelled following the results for Etna presented by Lesne et al. (2011):

$$x^{md,eq}_{d,H_2O} = 0.01 \cdot \left(\frac{\hat{f}_{H_2O}}{104.98}\right)^{\frac{1}{1.83}}, \tag{14}$$

where $\hat{f}_{H_2O} = f_{H_2O}/\mathbf{1}_{bar}$ is the non-dimensional water fugacity, f_{H_2O} is the water fugacity expressed in bars, and $\mathbf{1}_{bar}$ is the unity in bars. Following Holloway and Blank (1994) we approximate water fugacity in the pressure/temperature range of interest (<90 MPa, 1100–1200 °C) as:

$$f_{H_2O} = 0.9823(P_{H_2O}), \tag{15}$$

where P_{H_2O} is the partial pressure of water expressed in bars.

Similarly, the equilibrium dissolved CO_2 content is modelled as a function of carbon dioxide fugacity. This function has been derived from a 6th order polynomial fitting of the thermodynamical model presented by Allison et al. (2019):

$$x^{md,eq}_{d,CO_2} = -\left(a_6\hat{f}_{CO_2}\right)^6 + \left(a_5\hat{f}_{CO_2}\right)^5 - \left(a_4\hat{f}_{CO_2}\right)^4 + \left(a_3\hat{f}_{CO_2}\right)^3 - \left(a_2\hat{f}_{CO_2}\right)^2 + \left(a_1\hat{f}_{CO_2}\right) + a_0, \tag{16}$$

where $\hat{f}_{CO_2} = f_{CO_2}/\mathbf{1}_{bar}$ is a non-dimensional variable, f_{CO_2} is the fugacity of CO_2 expressed in bars, $a_6 = 1.59 \times 10^{-5}$, $a_5 = 1.81 \times 10^{-5}$, $a_4 = 1.755 \times 10^{-5}$, $a_3 = 1.33 \times 10^{-5}$, $a_2 = 5.93 \times 10^{-6}$, $a_1 = 5.32 \times 10^{-7}$, and $a_0 = 1.53 \times 10^{-5}$. Again following Holloway and Blank (1994), carbon dioxide fugacity can be approximated within the pressure and temperature

Table 1
Sunset Crater average composition of the melt inclusions used in the viscosity model.

Composition	
SiO_2	47.35
TiO_2	2.15
Al_2O_3	17.36
FeO	8.8
MnO	0.14
MgO	7.48
CaO	10.91
Na_2O	3.58
K_2O	0.98
P_2O_5	0.52
Tot.	99.27

ranges investigated in this work with another 6th order polynomial:

$$\hat{f}_{CO_2} = -\left(b_6\hat{P}_{CO_2}\right)^6 + \left(b_5\hat{P}_{CO_2}\right)^5 + \left(b_4\hat{P}_{CO_2}\right)^4 + \left(b_3\hat{P}_{CO_2}\right)^3 + \left(b_2\hat{P}_{CO_2}\right)^2 + \left(b_1\hat{P}_{CO_2}\right) + b_0, \quad (17)$$

where $\hat{P}_{CO_2} = P_{CO_2}/\mathbf{1}_{bar}$ is the non-dimensional partial pressure of carbon dioxide, P_{CO_2} is the partial pressure expressed in bars, $b_6 = 6.62 \times 10^{-4}$, $b_5 = 9.49 \times 10^{-4}$, $b_4 = 4.63 \times 10^{-4}$, $b_3 = 3.31 \times 10^{-3}$, $b_2 = 1.46 \times 10^{-2}$, $b_1 = 0.999999857$, and $b_0 = 2.32 \times 10^{-6}$.

2.2.3. Conduit wall friction

Because we are interested in simulating sub-Plinian to Plinian eruptions we expect to find high ascent velocities within the conduit, even before magma fragmentation. In such conditions, the liquid flow could be turbulent. In order to consider this possibility, we model the friction factor of the liquid phase f_{D_l} in Eqs. (3), (8) as a function of Reynolds number *Re*, which is calculated as

$$Re = \frac{\rho_l u_l 2r}{\mu_l}. \quad (18)$$

If the Reynolds number is <2000, we assume the flow is laminar, and adopt the widely used Hagen-Poiseuille's law by assuming

$$f_{D_l}^{laminar} = \frac{64}{Re}. \quad (19)$$

When *Re*> 3000, we approximate the friction factor for fully-developed turbulent flow based on the Colebrook equation (Colebrook, 1939; Fang et al., 2011). This equation combines experimental studies of turbulent flow in smooth and rough pipes. The validity of the Colebrook equation was reported to be in the range of $Re = 3000–10^8$ and $Rr = 0–0.05$, where *Rr* is the relative roughness of the pipe, which is the ratio of the surface roughness (i.e. is the average height of the surface irregularities within the pipe) and the diameter of the pipe.

This law is not convenient to use, however, because f_{D_l} is expressed implicitly, which requires several iterations to find a solution. For this reason, a number of approximate explicit counterparts have been proposed in the literature. Here we adopt the explicit approximation developed by Fang et al. (2011):

$$f_{D_l}^{turbulent} = 1.613\left[\ln\left(0.23Rr^{1.1007} - \frac{60.525}{Re^{1.1105}} + \frac{56.291}{Re^{1.0712}}\right)\right]^{-2}. \quad (20)$$

We assume the maximum relative roughness to be $Rr = 0.05$. In the transitional regime when $2000 \le Re \le 3000$, a linear interpolation between $f_{D_l}{}^{laminar}$ and $f_{D_l}{}^{turbulent}$ is used. Above the fragmentation level, gas-wall drag f_{D_g} is set to 0.03 as in Degruyter et al. (2012).

3. Numerical results

3.1. Application to the 1085 CE sub-Plinian eruptions at Sunset volcano

Sunset Crater is a ~290-m-high monogenetic scoria cone ~25 km northeast of Flagstaff, AZ. It is the youngest of roughly 600 scoria cones in the San Francisco Volcanic Field (Ort et al., 2008a). The eruption produced three lava flows that cover ~8 km^2, a scoria blanket up to 12 m thick covering an area of about 500 km^2, and minor spatter cones and ramparts (Ort et al., 2008a; Alfano et al., 2018). Sunset Crater produced a wide range of eruption styles including lava flows, fire-fountaining, and Strombolian to sub-Plinian explosive eruptions (Ort et al., 2008a, 2008b; Alfano et al., 2018). There were three main sub-Plinian explosions that erupted 0.12 to 0.33 km^3 of tephra (a total of 0.22 km^3 DRE), produced columns 20–30 km high, and were classified accordingly as VEI 3 (Alfano et al., 2018). Mass eruption rates (MER) were estimated to have been between ~5×10^6 and 1×10^8 kg/s and durations ranged from 20 to 90 min (Alfano et al., 2018).

Since the Sunset Crater eruption started as a fissure eruption, the plumbing system beneath the vent is likely to be more complicated than a simple cylindrical conduit geometry. Basaltic magmas in monogenetic volcanic fields commonly ascend through dykes in the deep plumbing system (Keating et al., 2008; Genareau et al., 2010; Valentine, 2012). Close to the surface in many cases, such as for the Sunset Crater eruption and any axisymmetric cinder cone, activity shifts from fissure-fed eruptions to eruptions supplied by cylindrical conduits which rapidly build near-axisymmetrical cinder cones (Keating et al., 2008; Genareau et al., 2010; Valentine, 2012). Harp and Valentine (2015) suggested that the transition from feeder dike to conduit occurs generally in the upper ~100 m of the crust. However, conduit geometry can occasionally extend several hundreds of meters or more into the subsurface (Valentine, 2012; Harp and Valentine (2015)).

Therefore, with the 1D conduit model described above we cannot simulate the entire magma ascent path. For this reason, we limit our analysis to the upper 500 m of the conduit, where the plumbing system is more likely to have cylindrical geometry. The presence of a dyke just beneath the cylindrical geometry can affect the overall magma ascent dynamics (Costa et al., 2009b; Aravena et al., 2018b), and we approximate this impact below in our analysis.

Since mass eruptions rates estimated for Sunset Crater are in the order of $10^7–10^8$ kg/s, we expect (for the typical conduit diameters in such systems) an average ascent velocity of tens of meters per seconds, suggesting that the ascent time in the last 500 m of the conduit would be <10 min. La Spina et al. (2016) estimated a crystallization time of ~2 h during magma ascent for several basaltic volcanoes. Therefore, our assumption of constant crystal content is appropriate for our case study.

Using published petrological analyses on Sunset Crater scoria samples and field observations (Allison, 2018; Alfano et al., 2018), we constrain many parameters for the magma ascent model at the inlet of the conduit. The temperature of the magma is ~1130 °C (Allison, 2018), the total dissolved water content is ~1.4 wt% (Allison, 2018), the total dissolved CO_2 content is ~4500 ppm (Allison, 2018), and the average total crystal content is ~33 vol%. The pressure of magma storage is between 300 and 500 MPa, suggesting a magma chamber located between 10 and 18 km (Allison, 2018). As discussed above, in our numerical simulation we consider only the upper 500 m of the conduit, assuming a magmatic pressure at that depth to be 15 MPa. We do not have robust constraints on the radius, and therefore vary it based on estimates from other similar systems. Keating et al. (2008) and Valentine (2012) suggest that conduit diameters in such systems range from a few tens of meters to ~100 m. We thus start with an initial value of 20 m and vary it in subsequent runs. The input parameters for this numerical simulation (from now on called "the reference simulation") are summarized in Table 2.

The numerical results for the reference simulation (Table 2) are reported in Fig. 3. Numerical solutions are obtained using a shooting technique, which consists of searching for the initial magma ascent velocity that leads to the boundary condition at the volcanic vent, which is either

Table 2
Input parameters chosen for the reference simulation and the range of values used for the sensitivity analysis.

Variable	Reference simulation	Sensitivity analysis
P	15 MPa	10–20 MPa
T	1130 °C	1100–1200 °C
r	20 m	10–30 m
$x_{d_{H2O}}$	1.4 wt%	1.0–2.0 wt%
$x_{d_{CO2}}$	4500 ppm	3000–9000 ppm
$\beta_{c,0}^{eq}$	0.33	0.10–0.45
L	500 m	500 m

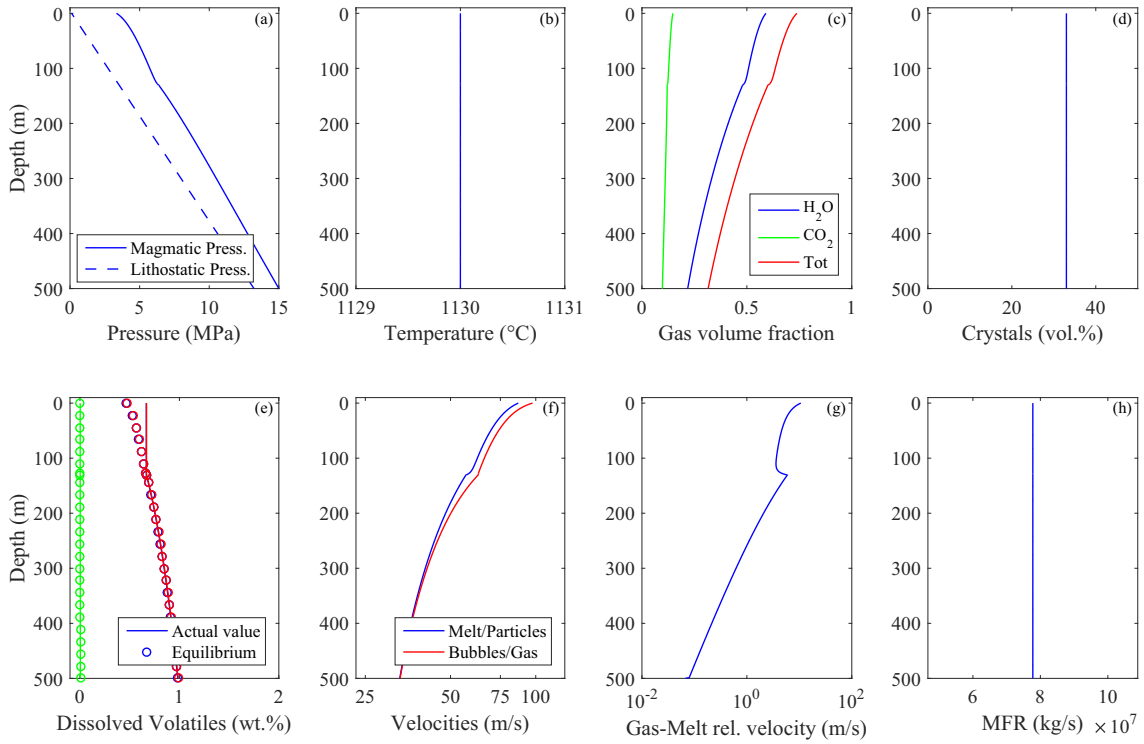

Fig. 3. Numerical results obtained from the conduit model for the 1085 CE Sunset Crater eruption. Pressure (a), temperature (b), gas volume fraction (c), crystal content (d), dissolved volatile contents (e), velocities (f), gas/melt relative velocity (g), and mass flow rate (h).

atmospheric pressure or the sonic condition (de' Michieli Vitturi et al., 2008). The mass flow rate calculated from this simulation is ~7.8 $\times$ 10^7 kg/s, within the estimated range for the sub-Plinian phases at Sunset Crater (Alfano et al., 2018), and any sub-Plinian eruption (Bonadonna and Costa, 2013). The ascent velocity at 500 m depth is ~34 m/s, meaning that it takes just a few seconds for magma to reach the surface. The ascent velocities of melt and bubbles are different in the shallow subsurface. The relative velocity between gas and melt increases with the decrease of depth, going from ~0.1 m/s at 500 m depth to ~10 m/s at fragmentation. Decoupling is mainly controlled by permeability, which is, in turn, a function of the gas volume fraction. The lower the gas volume fraction, the lower the permeability of the magma, resulting in a smaller gas-melt relative velocity (La Spina et al., 2017b). The two phases start to decouple significantly a few hundred meters below the vent. The open-system degassing associated with this decoupling, however, is not sufficient to prevent fragmentation, which occurs ~120 m below the vent.

3.2. Sensitivity analysis and general trends

For the basaltic systems of interest here, these input values span a reasonably wide range. We therefore extend beyond this reference simulation to conduct sensitivity analysis of the input parameters in order to demonstrate the influence of input parameters on some specific outputs. Here we focus on the following output: gas volume fraction at the vent, fragmentation depth, mass flow rate, and melt and gas velocity at the vent. The range of input parameters adopted for the sensitivity analysis are the following (Table 2): 10–20 MPa for the inlet pressure at 500 m depth, 1100–1200 °C for the magma temperature, 10–30 m for the radius of the conduit, 1.0–2.0 wt% for the total water content, 3000–9000 ppm for the total CO_2 content, and 10–45 vol% for the crystal content. Since we do not know the probability distribution of these input parameters, we assume a uniform distribution within the aforementioned ranges. The sensitivity analysis was performed on 10,000 different input scenarios using the DAKOTA toolkit (Design Analysis Kit for Optimization and Terascale Applications, (Adams et al., 2017), an open-source software developed at Sandia National Laboratories that provides an interface between analysis codes and iterative systems analysis methods such as uncertainty quantification, sensitivity analysis, optimization, and parameter estimation.

Fig. 4 shows the results of the sensitivity analysis. In the bottom panels of Fig. 4 we report with a frequency plot the variability of the output resulting from the sensitivity analysis. In the top panels we report the Sobol indexes for each of the output parameters. The Sobol index is a measure of how much the variability of an output parameter is related to the variability of a single input variable. More precisely, the Sobol index S_i^j of the variable χ_i for the output R_j is given by

$$S_i^j = \frac{Var\left[E\left(R_j \middle| \chi_i\right)\right]}{Var\left[R_j\right]}, \tag{21}$$

where E denotes the expected value, and Var is the variance. The bigger the Sobol index S_i^j, the more the variability in input χ_i is responsible for the observed variability in output R_j. In the bottom panels of Fig. 4 we report the frequency of the output resulting from the sensitivity analysis.

The results show that, within the ranges investigated, the gas volume fraction at the vent varies from 0.6 to 0.85, with a peak in frequency at ~0.75 (Fig. 4f). The variability in gas volume fraction at the vent and fragmentation depth are controlled mainly by variations in pressure at the inlet of the simulated conduit at 500 m depth (Fig. 4a,b). We highlight that, although these vent gas volume fractions appear too small to be consistent with the formation of a buoyant plume, the pressure at the vent is always greater than the atmospheric pressure (due to choked flow boundary condition at the vent). Therefore, once the gas/particle mixture equilibrates with the atmospheric pressure, the gas volume fraction becomes higher than 0.99, and therefore could form a buoyant plume. Fragmentation is mostly shallower than 500 m (Fig. 4g), but, for some combination of parameters (i.e. high water content and low inlet pressure), it can occur in the deeper feeding system.

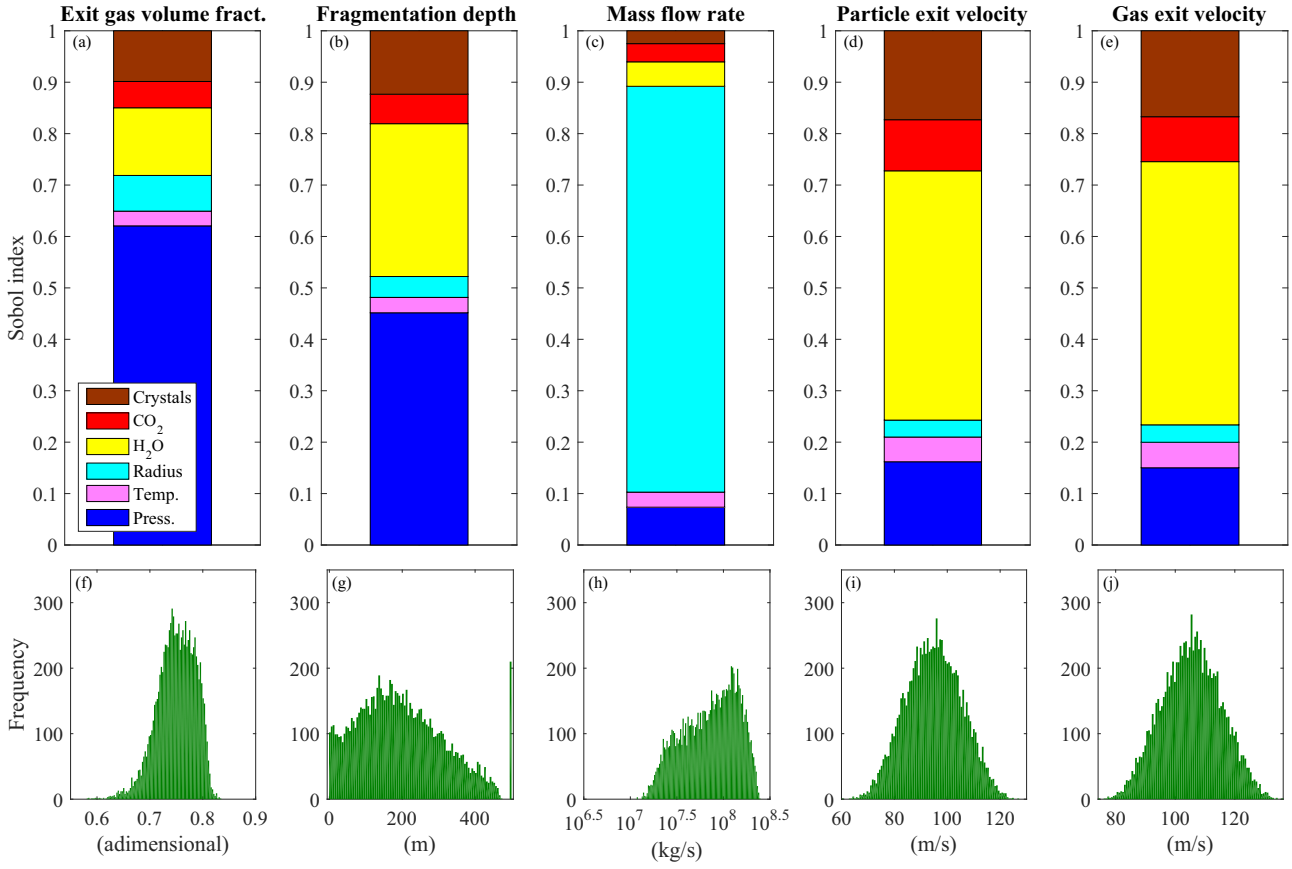

Fig. 4. Output of the sensitivity analysis. In the top panels we illustrate the Sobol indexes calculated using Eq. (20) for each of the output parameters: gas volume fraction at the vent, fragmentation depth, mass flow rate, particle and gas exit velocities. In the bottom panels, we report the frequency of the output resulting from the sensitivity analysis.

A comparison between gas and particle exit velocities shows that, on average, the gas exit velocities are ~10–20 m/s higher than particle velocities (Fig. 4i,j), with particle exit velocities ranging between 60 and 130 m/s, with a peak in frequency at ~90 m/s, and gas exit velocities ranging between 80 and 140 m/s, with a peak in frequency at ~110 m/s. The input parameters that exert the most control on exit velocities, in decreasing order of importance, are total water content, crystal content, pressure prescribed at the simulated conduit inlet at 500 m depth, and CO_2 content (Fig. 4d,e). Within the range considered here, magma temperature and conduit radius have secondary roles in controlling variations in exit velocities.

Mass flow rate varies between 10^7 and $10^{8.5}$ kg/s, with a peak at ~$10^{8.2}$ kg/s (Fig. 4h), always consistent with sub-Plinian eruption rates (Wilson and Walker, 1987; Mastin et al., 2009; Bonadonna and Costa, 2013). As expected, the variability in mass flow rate is controlled largely by variations in conduit radius (Fig. 4c). Other key factors are velocity and pressure at the vent.

Correlation plots show selected output variables as functions of given input parameters (Fig. 5 and Supplementary Figs. 1–5), further illustrating the ranges discussed above. Each red dot in Fig. 5 indicates one solution of the sensitivity analysis, whereas the blue lines represent the mean of the output parameters at a given input value. Decreasing the prescribed pressure at 500 m depth leads to increases in gas volume fraction at the vent and fragmentation depth (Fig. 5a,b). A decrease in pressure at the inlet of the conduit at 500 m depth results in a decrease in pressure all along the conduit, promoting further exsolution and expansion of volatiles, favouring deeper magma fragmentation. This is a somewhat counter-intuitive result, as it suggests that finer ash might be produced due to comminution with decreasing pressure (Dufek et al., 2012). Moreover, a decrease in conduit pressure results in a decrease in mass flow rate and in exit velocities (Supplementary Figs. 3–5). Again, we observe a strong correlation between the radius of the conduit and the mass flow rate (Fig. 5c). Furthermore, particle exit velocity decreases with increasing crystal content (Fig. 5d), due to the increased viscosity. This increase also impacts gas exit velocity, because the two phases are never fully decoupled (the gas-particle relative velocity at the vent is always ~10–20 m/s). Moreover, an increase in volatile content produces an increase in particle exit velocity (Fig. 5e,f). The fragmentation depth is not significantly affected by the different crystal contents investigated here, even though a slight decrease in the fragmentation depth can be observed as the crystal content increases (Supplementary Fig. 2).

For the simulations with a 20 m conduit radius resulting in a choked flow condition at the vent, Fig. 6 shows the pressure at the vent versus gas volume fraction at the vent. The colour of the symbols indicates the particle exit velocity, while the size of the symbol reflects the mass flow rate. Velocity and mass flow rate are the key input parameters for plume models (Costa et al., 2016), and therefore gaining an understanding of their relationship with subsurface dynamics is desirable. For example, lower pressure at the vent corresponds to higher gas mass fraction, which is a direct consequence of instantaneous exsolution assumed in our simulations. Moreover, higher pressure at the vent results in higher exit velocity, which is caused by an increase in local pressure gradient close to the vent. This increase in exit velocity may result in an increase in mass flow rate. However, an increase in the gas volume fraction at the vent corresponds, in general, to a lower mass flow rate. This decrease is caused by the corresponding decrease in inlet pressure, which, as we discussed previously, leads to an increase in gas volume fraction at the vent, but also to a decrease in exit velocity such that only low to moderate velocities are represented. Therefore, the highest

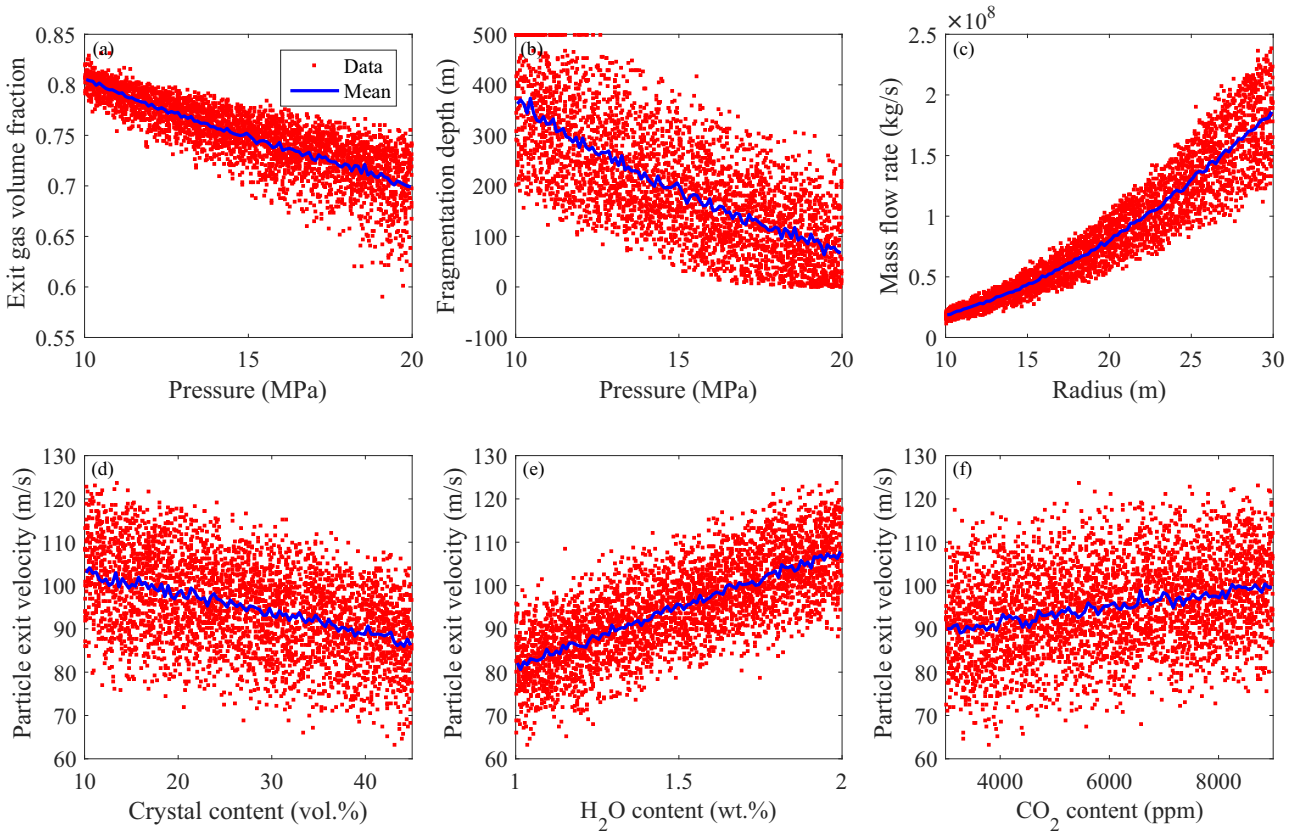

Fig. 5. Correlation plots of the output parameters computed from the sensitivity analysis as function of some of the input parameters. Each marker represents a different simulation, whereas the blue lines represent the mean of the output parameters at a given input value. For a fixed value of the input parameters on the x-axis, the vertical spreading of results depends on variations in the other input parameters.

mass flow rates generally fall along the leftmost edge of the cloud of points, representing the highest vent pressure for any given vent gas volume fraction.

3.3. Approximation of the transient behaviour of the system

The sensitivity analysis shows that, during an eruption, changing conduit inlet pressure at depth plays a key role in controlling the variability in the output values investigated here, with a key observation that decreasing pressure at the inlet of the simulated conduit (500 m depth) increases fragmentation depth and gas volume fraction at the vent, and decreases mass flow rate. This decrease in pressure at the conduit inlet will occur if the magma chamber empties during the course of an eruption.

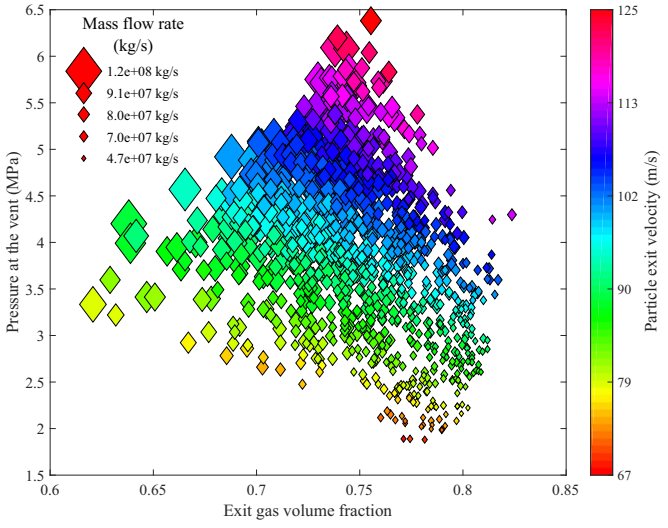

Fig. 6. Correlation of some output parameters at the vent, which are the key input parameters for plume models.

In order to analyse this scenario further, we approximate the transient behaviour of the system by generating a sequence of multiple steady-state runs for which the inlet pressure was progressively lowered, starting with the reference simulation conditions. Decreasing pressure at 500 m produces a decrease in pressure all along the conduit, generating further exsolution and gas expansion. This, in turn, allows fragmentation to occur progressively deeper in the conduit, even though ascent velocities and mass flow rate decrease under the same conditions. Results for inlet pressures of 15 (blue lines), 10 (green lines), 5 (red lines), and 2.5 MPa (black lines) are shown in Fig. 7. As we can see, although the pressure at 500 m decreases from 15 to 2.5 MPa, magma is still able to reach the surface to create an explosive eruption, although the mass flow rate decreases by almost an order of magnitude from 8.0×10^7 to 1.1×10^7 kg/s. This pressure decrease within the conduit could produce instability of the conduit walls, generating a collapse of the conduit itself.

To test the stability of the conduit walls during this pressure decrease, we compare the minimum pressure required to support a stable conduit, predicted by the Mohr–Coulomb collapse criteria (Al-Ajmi and Zimmerman, 2006; Aravena et al., 2017, 2018a), against the pressure profile within the conduit. In Fig. 7a the black dashed line represents this Mohr-Coulomb pressure threshold. When the inlet pressure at 500 m drops to 2.5 MPa, the pressure at 500 m depth reached the collapse threshold, which means that the upper part of the conduit should collapse. A corresponding collapse of the conduit would create an

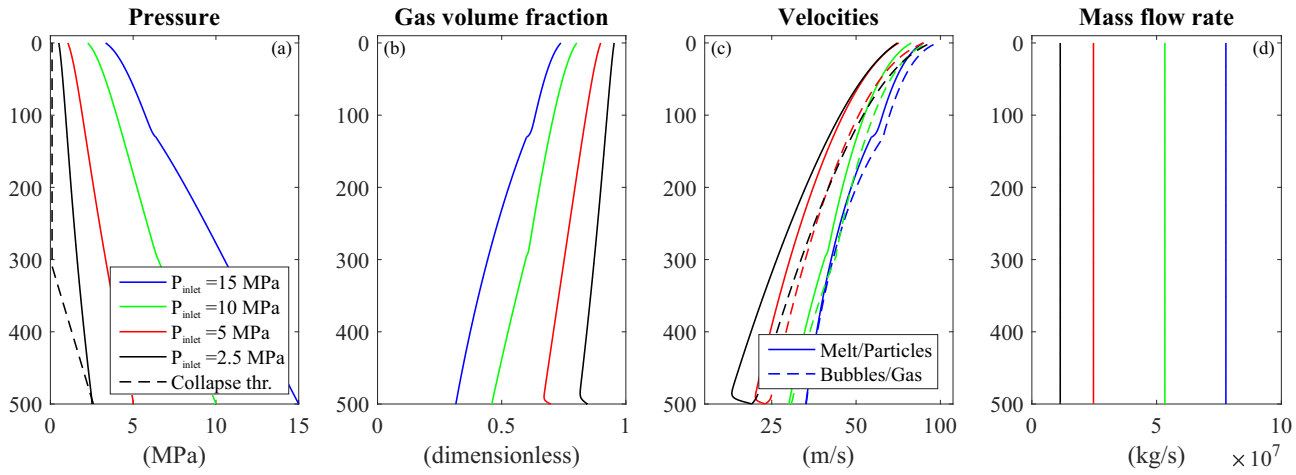

Fig. 7. Approximation of the transient behaviour of the system, simulating the pressure decrease due to the emptying of a magma chamber. Here we plot numerical solutions obtained assuming an inlet pressure of 15 (blue lines), 10 (green lines), 5 (red lines), and 2.5 MPa (black lines) respectively. The black dashed line in panel (a) represents the Mohr-Coulomb pressure threshold for conduit collapse.

overburden pressure, possibly leading to the end of a particular explosive eruption phase. The instability of a volcanic conduit during a sub-Plinian eruption may thus cause episodic conduit collapse events and intermittent discharge rates, as has been recognized for more silicic magmas (Bursik, 1993; Cioni et al., 2003) but not, until now, suggested for basaltic magmas. The presence of lithics in the tephra deposits (Alfano et al., 2018) suggests that this hypothesis is feasible. Although there is a low lithic content in the tephra fallout (<5 vol%), this amount would be sufficient to fill a 500 m deep cylindrical conduit with a 20 m radius. The main sub-Plinian explosions at Sunset Crater volcano erupted ~0.1–0.3 km^3 of tephra, which results in $<10^7$ m^3 of lithics, whereas the volume of the conduit would be ~5×10^5 m^3, supporting the hypothesis of conduit collapse.

We propose this mechanism to explain the duration of individual explosive phases at Sunset Crater and other highly-explosive basaltic eruptions. Below we explore this scenario in further detail.

3.4. Estimation of the magma chamber volume

We proceed by assuming that the eruptions are fed by a magma chamber in the mid-crust and explore the conditions and timescales under which eruptive pauses and/or the end of the eruption are caused by the collapse of the conduit walls. Following Woods and Koyaguchi (1994), Melnik (2000) and Melnik and Sparks (2005), we can estimate the temporal evolution of pressure in a magma chamber with the following equation:

$$\frac{\partial p_{ch}}{\partial t} = \frac{4EK}{\rho V_{ch}(3K+4E)}(Q_{in} - Q_{out}), \tag{22}$$

where p_{ch} is the pressure of the magma chamber, E is the elastic modulus of the surrounding rock, K and ρ are the bulk modulus and the average density of the magma, respectively, V_{ch} is the volume of the chamber, and Q_{in} and Q_{out} are the mass flow rates into and out of the magma chamber, respectively. For our calculations, we assume an elastic modulus $E = 2 \times 10^{10}$ Pa, a bulk modulus of $K = 10^{10}$ Pa, and an average density $\rho = 2700$ kg m^{-3} (Tait et al., 1989). Furthermore, we assume that influx of new magma into the magma chamber is negligible and thus set $Q_{in} = 0$.

Since the pressure profile is not constant throughout the conduit, the pressure change we simulated at 500 m does not correspond directly to the same change in pressure at depth required in Eq. (22). A lower bound for the pressure at 15 km (the possible depth of the magma chamber, according to estimations from Allison, 2018) can be obtained assuming magmastatic conditions, because if the pressure gradient is lower than the magmastatic value, magma would not be able to ascend. At magmastatic conditions, the pressure change at 15 km is exactly equal to the pressure change at 500 m. This means that a pressure change of 10 MPa at 500 m corresponds to a pressure change of 10 MPa at 15 km depth.

An upper bound for the pressure at 15 km can be obtained by extending the numerical domain beyond 500 m to a 15 km cylindrical conduit. The presence of a dyke-like geometry in the deeper feeding system can alter the pressure profile at depth, but it is possible to show that for such a geometry the pressure gradient is lower than that resulting from a constant radius cylindrical geometry. Following de' Michieli Vitturi et al. (2010), we model the dyke geometry as an elongated ellipse with width $2R_A$ and length $2R_B$ where $R_A < R_B$, and the viscous force for laminar flow, which is the case for magma rising in the deeper portions of the conduit, can be written as

$$F_D = 4\mu_l \frac{R_A^2 + R_B^2}{R_A^2 R_B^2} u_l.$$

For fixed values of viscosity μ_l and ascent velocity u_l, the viscous forces exerted in a cylindrical conduit with diameter equal to the width of the dyke ($R = R_A$) are F_C. We thus can compare the viscous forces in the two geometries by writing the ratio of viscous forces in a dyke to viscous forces in a cylindrical conduit (for which $R = R_A$):

$$\frac{F_D}{F_C} = \frac{1}{2}\left(\frac{R_A^2}{R_B^2} + 1\right) < 1.$$

This means that the viscous force is smaller for a dyke with width R_A than for a conduit with radius R_A. If we also consider that, due to the larger cross-sectional area, ascent velocity is expected to be lower in the dyke than in the conduit portion, the viscous force in the dyke may be even smaller.

We now remind the reader that the larger the viscous force, the larger the pressure gradient required to overcome this force and drive magma ascent in the conduit or dyke. In other words, for equivalent viscosities and ascent rates, a 15-km-long cylinder must have a larger pressure gradient than a system with a dyke-to-cylinder transition at 500 m, and thus the cylinder must also have greater pressure at depth. We also note here that losses associated with a constriction at a dyke-conduit interface are insignificant in comparison to the viscous forces described here, and thus they can be ignored in this comparative analysis. This

comparison justifies our assumption that the pressure gradient in a pure cylindrical geometry up to 15 km depth represents an upper bound for the pressure gradient and pressure at depth in a dyke-conduit system.

For a cylindrical conduit extended down to 15 km, we obtained a pressure at depth of 440 MPa, when pressure at 500 m is 15 MPa, whereas 10 MPa at 500 m corresponds to 415 MPa at 15 km, and analogously for pressures at other depths. Thus, a pressure change of 10 MPa at 500 m corresponds to a pressure change of 35 MPa at 15 km depth. We therefore constrain the pressure change at 15 km needed in Eq. (21) to be between the lower and upper bounds described above.

Using these approximations and the eruption rates computed from the approximation of the transient behaviour of the system, we calculate eruption duration for different chamber volumes. Fig. 8 shows variations in pressure as a function of time assuming $V_{ch} = 1$ km^3 (blue lines), 10 km^3 (red lines) and 100 km^3 (black lines). On the left *y*-axis, we report the pressure at the inlet of the conduit, whereas on the right *y*-axis we report the corresponding pressure at 15 km assuming a cylindrical conduit. The solid lines are the results obtained assuming a 15 km cylindrical conduit, whereas the dashed lines are those assuming magmastatic conditions. Furthermore, alongside the symbols we indicate the mass flow rate calculated from the approximation of the transient behaviour of the system. For each chamber volume, the coloured region highlights where the evolution of pressure as a function of time lies. The results demonstrate that the volume of the chamber significantly affects the duration of the eruption, such that the duration of the eruption is linearly proportional to the chamber volume. The published durations of the Sunset Crater sub-Plinian phases range from 20 to 90 min (Alfano et al., 2018). Comparing these estimates with our calculations, we constrain the magma chamber to be on the order of tens of km^3. The main sub-Plinian explosions at Sunset Crater volcano erupted 0.1–0.3 km^3 of tephra, which represents ~1% of a magma chamber that is ~10 km^3. This is an order of magnitude greater than small but frequent basaltic eruptions from volcanoes in Hawaii and Iceland, which typically erupt ~0.1% of the magma chamber volume (Sigmundsson et al., 1992; Pietruszka and Garcia, 1999; Garcia et al., 2000; Parfitt and Wilson, 2008). This magnitude of erupted vs. chamber volume is more consistent with that of silicic sub-Plinian eruptions, such as the 1631 sub-Plinian eruption at Somma-Vesuvius (Barberi et al., 1981; Rosi et al., 1993). Smith and Shaw (1973, 1978) estimated volumes of silicic magma chambers based on ejected volumes, caldera extent, and other area criteria. These volume estimates indicated that no more than approximately one-tenth of the chamber volume can be erupted during any explosive activity (Smith, 1979).

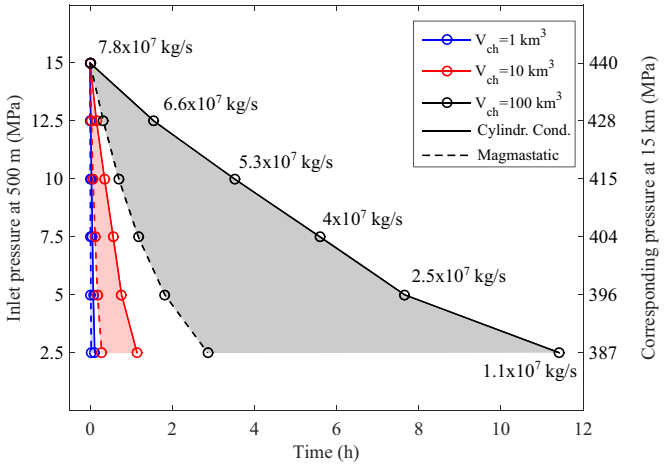

Fig. 8. Variation of the pressure and mass eruption rate with time for different chamber volumes: 1 km^3 (blue lines), 10 km^3 (red lines) and 100 km^3 (black lines). The solid lines are the results obtained assuming a 15 km cylindrical conduit, whereas the dashed lines are those assuming magmastatic conditions.

The different ratio of the erupted volume compared to the magma chamber volume between highly explosive basaltic eruptions and basaltic activity with lower explosivity (such as lava flows or low-intensity fire-fountaining) can be related to the efficiency of gas/melt decoupling and to the different mechanism causing cessation of the eruption. The slow ascent of small-scale basaltic activity will favour gas/melt decoupling, whereas it will be inhibited for fast ascending magmas, such as in highly explosive basaltic explosive eruptions. Furthermore, as soon as gas efficiently decouples from magma, ascent will slow and, eventually, the eruption will cease. On the other hand, if decoupling is not significant, such as for the Sunset Crater eruption, then the eruption may continue until conduit underpressure causes the wall of the conduit to collapse. For these reasons, we suggest that highly explosive basaltic eruptions can evacuate about 1% of the chamber volume, which is one order of magnitude higher than small basaltic eruptions.

4. Conclusions

In this work we investigate the dynamics of magma ascent at shallow depths for the 1085 CE Sunset Crater basaltic sub-Plinian eruption, using a 1D steady-state magma ascent model for cylindrical conduits. Field observations and petrological analyses of Sunset Crater scoria samples from previous work were adopted to constrain some input parameters for the conduit model described here. Notwithstanding the several assumptions adopted here (such as constant radius of the conduit, isothermal conditions, constant crystal content, instantaneous exsolution, pressure equilibrium between phases), using these initial conditions, we successfully simulate basaltic sub-Plinian eruptions consistent with those at Sunset Crater. We also find that a key parameter controlling the variability in the output parameters, such as gas volume fraction at the vent and fragmentation depth, is the pressure at depth. In particular, we find that a decrease in this pressure will increase the fragmentation depth and decrease mass eruption rate.

We also show that a continuous decrease in this pressure, consistent with the emptying of a magma chamber or storage zone, may lead to the collapse of the upper part of the conduit, creating overburden sufficient to end an individual explosive phase. More generally, our results indicate that the collapse of the conduit is something feasible for basaltic Plinian and sub-Plinian eruptions, and that it could be one key mechanism explaining the duration of individual explosive phases. Using this conceptual model, we constrain the volume of the magma chamber at Sunset Crater to be on the order of 10 km^3. Comparing the estimated storage volume with the erupted ones, we infer that ~1% of the magma chamber volume was erupted during each sub-Plinian phase, which is one order of magnitude higher than small basaltic eruptions. Finally, we suggest that this result, which relies on general mechanisms occurring in all sub-Plinian and Plinian basaltic eruptions, can be generalised to similar highly basaltic explosive eruptions.

Numerical results shown here demonstrate that numerical models constrained by petrological and other field observations are invaluable tools in understanding magma ascent dynamics, particularly for highly explosive basaltic eruptions for which we do not have any direct observation of eruption dynamics. A clearer understanding of the complex non-linear conduit processes occurring during these basaltic explosive systems is of profound importance in assessing the hazard associated with these volcanoes.

Acknowledgments

Sensitivity analyses were performed on the ARCHER National Supercomputing Service (UK).

The executable of the conduit model used in this work can be downloaded from the link bit.ly/MAMMA_CODE_v0d2.

We gratefully acknowledge funding support from RCUK NERC DisEqm project (NE/N018575/1) and NSF EAR Grant 1642569.

Finally, we gratefully acknowledge the contribution of focused and detailed review comments from Greg Valentine and two anonymous reviewers, which significantly improved this manuscript.

Appendix A. Supplementary data

Supplementary data to this article can be found online at https://doi.org/10.1016/j.jvolgeores.2019.08.001.

References

Adams, B.M., Ebeida, M.S., Eldred, M.S., Geraci, G., Jakeman, J.D., Maupin, K.A., et al., 2017. DAKOTA, a Multilevel Parallel Object-Oriented Framework for Design Optimization, Parameter Estimation, Uncertainty Quantification, and Sensitivity Analysis Version 6.6 User's Manual. (*Technical report*, SAND2014-4633).

Agostini, C., Fortunati, A., Arzilli, F., Landi, P., Carroll, M.R., 2013. Kinetics of crystal evolution as a probe to magmatism at Stromboli (Aeolian Archipelago, Italy). Geochim. Cosmochim. Acta 110, 135–151. https://doi.org/10.1016/j.gca.2013.02.027.

Al-Ajmi, A.M., Zimmerman, R.W., 2006. Stability analysis of vertical boreholes using the Mogi—Coulomb failure criterion. Int. J. Rock Mech. Min. Sci. 43, 1200–1211. https://doi.org/10.1016/j.ijrmms.2006.04.001.

Alfano, F., Pioli, L., Clarke, A., Ort, M., Roggensack, K., Self, S., 2014. Evidence of a complex shallow reservoir network from micro-textural observations of the scoria products of the 1085 AD Sunset Crater eruption. AGU Fall Meeting Abstracts http://adsabs.harvard.edu/abs/2014AGUFM.V21B4748A.

Alfano, F., Ort, M.H., Pioli, L., Self, S., Hanson, S.L., Roggensack, K., et al., 2018. The sub-Plinian monogenetic basaltic eruption of Sunset Crater, Arizona, USA. Bull. Geol. Soc. Am. https://doi.org/10.1130/B31905.1.

Allison, C.M., 2018. Highly Explosive Mafic Volcanism: The Role of Volatiles. *PhD thesis*. Arizona State University (226 pages).

Allison, C.M., Roggensack, K., Clarke, A.B., 2019. H_2O–CO_2 solubility in alkali-rich mafic magmas: new experiments at mid-crustal pressures. Contrib. Mineral. Petrol. 174 (7), 58. https://doi.org/10.1007/s00410-019-1592-4.

Aravena, Á., de' Michieli Vitturi, M., Cioni, R., Neri, A., 2017. Stability of volcanic conduits during explosive eruptions. J. Volcanol. Geotherm. Res. 339, 52–62. https://doi.org/10.1016/j.jvolgeores.2017.05.003.

Aravena, Á., Cioni, R., de' Michieli Vitturi, M., Neri, A., 2018a. Conduit stability effects on intensity and steadiness of explosive eruptions. Sci. Rep. 8, 4125. https://doi.org/10.1038/s41598-018-22539-8.

Aravena, Á., Cioni, R., de' Michieli Vitturi, M., Pistolesi, M., Ripepe, M., Neri, A., 2018b. Evolution of conduit geometry and eruptive parameters during effusive events. Geophys. Res. Lett. 45, 7471–7480. https://doi.org/10.1029/2018GL077806.

Arzilli, F., Agostini, C., Landi, P., Fortunati, A., Mancini, L., Carroll, M., 2015. Plagioclase nucleation and growth kinetics in a hydrous basaltic melt by decompression experiments. Contrib. Mineral. Petrol. 170, 1–16. https://doi.org/10.1007/s00410-015-1205-9.

Barberi, F., Bizouard, H., Clocchiatti, R., Metrich, N., Santacroce, R., Sbrana, A., 1981. The Somma-Vesuvius magma chamber: a petrological and volcanological approach. Bull. Volcanol. 44 (3), 295–315. https://doi.org/10.1007/bf02600566.

Behncke, B., Branca, S., Corsaro, R.A., De Beni, E., Miraglia, L., Proietti, C., 2014. The 2011–2012 summit activity of Mount Etna: birth, growth and products of the new SE crater. J. Volcanol. Geotherm. Res. 270, 10–21. https://doi.org/10.1016/j.jvolgeores.2013.11.012.

Bonadonna, C., Costa, A., 2013. Plume height, volume, and classification of explosive volcanic eruptions based on the Weibull function. Bull. Volcanol. 75 (8), 742. https://doi.org/10.1007/s00445-013-0742-1.

Branca, S., Del Carlo, P., 2005. Types of eruptions of Etna volcano AD 1670–2003: implications for short-term eruptive behaviour. Bull. Volcanol. 67, 732–742. https://doi.org/10.1007/s00445-005-0412-z.

Brown, G.O., 2003. The history of the Darcy-Weisbach equation for pipe flow resistance. Environmental and Water Resources History, 34–43 https://doi.org/10.1061/40650(2003)4.

Bursik, M., 1993. Subplinian eruption mechanisms inferred from volatile and clast dispersal data. J. Volcanol. Geotherm. Res. 57, 57–70. https://doi.org/10.1016/0377-0273(93)90031-l.

Campagnola, S., Romano, C., Mastin, L.G., Vona, A., 2016. Confort 15 model of conduit dynamics: applications to Pantelleria Green Tuff and Etna 122 BC eruptions. Contrib. Mineral. Petrol. 171 (6), 60. https://doi.org/10.1007/s00410-016-1265-5.

Cioni, R., Sulpizio, R., Garruccio, N., 2003. Variability of the eruption dynamics during a subplinian event: the Greenish Pumice eruption of Somma–Vesuvius (Italy). J. Volcanol. Geotherm. Res. 124, 89–114. https://doi.org/10.1016/s0377-0273(03)00070-2.

Cioni, R., Pistolesi, M., Rosi, M., 2015. Plinian and subplinian eruptions. In: Sigurdsson, H., Houghton, B., McNutt, S., Rymer, H., Stix, J. (Eds.), The Encyclopedia of Volcanoes, Second edition Elsevier, pp. 519–535 https://doi.org/10.1016/b978-0-12-385938-9.00029-8.

Clarke, A.B., 2013. Unsteady explosive activity: Vulcanian eruptions. In: Fagents, S.A., Gregg, T.K., Lopes, R.M. (Eds.), Modeling Volcanic Processes. Cambridge Univ. Press, pp. 129–152.

Clarke, A.B., Ongaro, T., Belousov, A., 2015. Vulcanian Eruptions. In: Sigurdsson, H., Houghton, B., McNutt, S., Rymer, H., Stix, J. (Eds.), The Encyclopedia of Volcanoes. Elsevier, pp. 505–518 https://doi.org/10.1016/b978-0-12-385938-9.00028-6.

Colebrook, F., 1939. Turbulent flow in pipes with particular reference to the transition region between the smooth and rough pipe laws. J. Inst. Civ. Eng. (4), 14–25 https://doi.org/10.1680/ijoti.1939.13150.

Coltelli, M., Del Carlo, P., Vezzoli, L., 1998. Discovery of a Plinian basaltic eruption of Roman age at Etna volcano, Italy. Geology 26, 1095–1098. https://doi.org/10.1130/0091-7613(1998)026<1095:doapbe>2.3.co;2.

Costa, A., 2005. Viscosity of high crystal content melts: dependence on solid fraction. Geophys. Res. Lett. 32, L22308. https://doi.org/10.1029/2005GL024303.

Costa, A., Melnik, O., Vedeneeva, E., 2007. Thermal effects during magma ascent in conduits. J. Geophys. Res. Solid Earth 112 (B12). https://doi.org/10.1029/2007JB004985.

Costa, A., Caricchi, L., Bagdassarov, N., 2009a. A model for the rheology of particle-bearing suspensions and partially molten rocks. Geochem. Geophys. Geosyst. 10, Q03010. https://doi.org/10.1029/2008gc002138.

Costa, A., Sparks, R.S.J., Macedonio, G., Melnik, O., 2009b. Effects of wall-rock elasticity on magma flow in dykes during explosive eruptions. Earth Planet. Sci. Lett. 288, 455–462. https://doi.org/10.1016/j.epsl.2009.10.006.

Costa, A., Suzuki, Y.J., Cerminara, M., Devenish, B.J., Ongaro, T.E., Herzog, M., et al., 2016. Results of the eruptive column model inter-comparison study. J. Volcanol. Geotherm. Res. 326, 2–25. https://doi.org/10.1016/j.jvolgeores.2016.01.017.

Costantini, L., Bonadonna, C., Houghton, B.F., Wehrmann, H., 2009. New physical characterization of the Fontana Lapilli basaltic Plinian eruption, Nicaragua. Bull. Volcanol. 71 (3), 337. https://doi.org/10.1007/s00445-008-0227-9.

Costantini, L., Houghton, B.F., Bonadonna, C., 2010. Constraints on eruption dynamics of basaltic explosive activity derived from chemical and microtextural study: the example of the Fontana Lapilli Plinian eruption, Nicaragua. J. Volcanol. Geotherm. Res. 189 (3), 207–224. https://doi.org/10.1016/j.jvolgeores.2009.11.008.

Degruyter, W., Bachmann, O., Burgisser, A., Manga, M., 2012. The effects of outgassing on the transition between effusive and explosive silicic eruptions. Earth Planet. Sci. Lett. 349, 161–170. https://doi.org/10.1016/j.epsl.2012.06.056.

de' Michieli Vitturi, M., Clarke, A.B., Neri, A., Voight, B., 2008. Effects of conduit geometry on magma ascent dynamics in dome-forming eruptions. Earth Planet. Sci. Lett. 272 (3–4), 567–578. https://doi.org/10.1016/j.epsl.2008.05.025.

de' Michieli Vitturi, M., Clarke, A.B., Neri, A., Voight, B., 2010. Transient effects of magma ascent dynamics along a geometrically variable dome-feeding conduit. Earth Planet. Sci. Lett. 295 (3–4), 541–553. https://doi.org/10.1016/j.epsl.2010.04.029.

Di Genova, D., Kolzenburg, S., Wiesmaier, S., Dallanave, E., Neuville, D.R., Hess, K.U., Dingwell, D.B., 2017. A compositional tipping point governing the mobilization and eruption style of rhyolitic magma. Nature 552, 235–238. https://doi.org/10.1038/nature24488.

Dobran, F., 1992. Nonequilibrium flow in volcanic conduits and application to the eruptions of Mt. St. Helens on May 18, 1980, and Vesuvius in AD 79. J. Volcanol. Geotherm. Res. 49 (3–4), 285–311. https://doi.org/10.1016/0377-0273(92)90019-A.

Dufek, J., Manga, M., Patel, A., 2012. Granular disruption during explosive volcanic eruptions. Nat. Geosci. 5 (8), 561. https://doi.org/10.1038/ngeo1524.

Fang, X., Xu, Y., Zhou, Z., 2011. New correlations of single-phase friction factor for turbulent pipe flow and evaluation of existing single-phase friction factor correlations. Nucl. Eng. Des. 241, 897–902. https://doi.org/10.1016/j.nucengdes.2010.12.019.

Garcia, M.O., Pietruszka, A.J., Rhodes, J.M., Swanson, K., 2000. Magmatic processes during the prolonged Pu'u'O'o eruption of Kilauea Volcano, Hawaii. J. Petrol. 41 (7), 967–990. https://doi.org/10.1093/petrology/41.7.967.

Genareau, K., Valentine, G. A., Moore, G. & Hervig, R. L (2010). Mechanisms for transition in eruptive style at a monogenetic scoria cone revealed by microtextural analyses (Lathrop Wells volcano, Nevada, USA). Bull. Volcanol., 72, 593–607. doi:https://doi.org/10.1007/s00445-010-0345-z.

Giordano, D., 2019. Advances in the rheology of natural multiphase silicate melts: import for magma transport and lava flow emplacement. Ann. Geophys. 61, 65. https://doi.org/10.4401/ag-7859.

Giordano, D., Dingwell, D., 2003. Viscosity of hydrous Etna basalt: implications for Plinian-style basaltic eruptions. Bull. Volcanol. 65, 8–14. https://doi.org/10.1007/s00445-002-0233-2.

Giordano, D., Russell, J.K., Dingwell, D.B., 2008. Viscosity of magmatic liquids: a model. Earth Planet. Sci. Lett. 271, 123–134. https://doi.org/10.1016/j.epsl.2008.03.038.

Gonnermann, H.M., Manga, M., 2003. Explosive volcanism may not be an inevitable consequence of magma fragmentation. Nature 426, 432–435. https://doi.org/10.1038/nature02138.

Gonnermann, H.M., Manga, M., 2013. Dynamics of magma ascent in the volcanic conduit. In: Fagents, S.A., Gregg, T.K., Lopes, R.M. (Eds.), Modeling Volcanic Processes. Cambridge Univ. Press, pp. 55–84 https://doi.org/10.1017/cbo9781139021562.004.

Harp, A.G., Valentine, G.A., 2015. Shallow plumbing and eruptive processes of a scoria cone built on steep terrain. J. Volcanol. Geotherm. Res. 294, 37–55. https://doi.org/10.1016/j.jvolgeores.2015.02.008.

Holloway, J.R., Blank, J.G., 1994. Application of experimental results to COH species in natural melts. Rev. Mineral. 30, 187–230.

Houghton, B.F., Gonnermann, H.M., 2008. Basaltic explosive volcanism: constraints from deposits and models. Chem. Erde-Geochem. 68 (2), 117–140. https://doi.org/10.1016/j.chemer.2008.04.002.

Keating, G. N., Valentine, G. A., Krier, D. J. & Perry, F. V (2008). Shallow plumbing systems for small-volume basaltic volcanoes. Bull. Volcanol., 70, 563–582. doi:https://doi.org/10.1007/s00445-007-0154-1.

Kozono, T., Koyaguchi, T., 2009. Effects of relative motion between gas and liquid on 1-dimensional steady flow in silicic volcanic conduits: 1. An analytical method. J. Volcanol. Geotherm. Res. 180, 21–36. https://doi.org/10.1016/j.jvolgeores.2008.11.006.

La Spina, G., de' Michieli Vitturi, M., Romenski, E., 2014. A compressible single-temperature conservative two-phase model with phase transitions. Int. J. Numer. Methods Fluids 76, 282–311. https://doi.org/10.1002/fld.3934.

La Spina, G., Burton, M., de' Michieli Vitturi, M., 2015. Temperature evolution during magma ascent in basaltic effusive eruptions: a numerical application to Stromboli volcano. Earth Planet. Sci. Lett. 426, 89–100. https://doi.org/10.1016/j.epsl.2015.06.015.

La Spina, G., Burton, M., de' Michieli Vitturi, M., Arzilli, F., 2016. Role of syn-eruptive plagioclase disequilibrium crystallization in basaltic magma ascent dynamics. Nat. Commun. 7, 13402. https://doi.org/10.1038/ncomms13402.

La Spina, G., de' Michieli Vitturi, M., Clarke, A.B., 2017a. Transient numerical model of magma ascent dynamics: application to the explosive eruptions at the Soufrière Hills Volcano. J. Volcanol. Geotherm. Res. 336, 118–139. https://doi.org/10.1016/j.jvolgeores.2017.02.013.

La Spina, G., Polacci, M., Burton, M., de' Michieli Vitturi, M., 2017b. Numerical investigation of permeability models for low viscosity magmas: application to the 2007 Stromboli effusive eruption. Earth Planet. Sci. Lett. 473, 279–290. https://doi.org/10.1016/j.epsl.2017.06.013.

Lavallée, Y., Dingwell, D.B., Johnson, J.B., Cimarelli, C., Hornby, A.J., Kendrick, J.E., Rhodes, E., 2015. Thermal vesiculation during volcanic eruptions. Nature 528 (7583), 544. https://doi.org/10.1038/nature16153.

Lesne, P., Scaillet, B., Pichavant, M., Iacono-Marziano, G., Beny, J.M., 2011. The H_2O solubility of alkali basaltic melts: an experimental study. Contrib. Mineral. Petrol. 162, 133–151. https://doi.org/10.1007/s00410-010-0588-x.

Llewellin, E.W., Manga, M., 2005. Bubble suspension rheology and implications for conduit flow. J. Volcanol. Geotherm. Res. 143, 205–217. https://doi.org/10.1016/j.jvolgeores.2004.09.018.

Llewellin, E.W., Mader, H.M., Wilson, S.D.R., 2002. The constitutive equation and flow dinamics of bubbly magmas. Geophys. Res. Lett. 29, 2170. https://doi.org/10.1029/2002GL015697.

Macedonio, G., Neri, A., Martí, J., Folch, A., 2005. Temporal evolution of flow conditions in sustained magmatic explosive eruptions. J. Volcanol. Geotherm. Res. 143 (1–3), 153–172. https://doi.org/10.1016/j.jvolgeores.2004.09.015.

Mader, H.M., Llewellin, E.W., Mueller, S.P., 2013. The rheology of two-phase magmas: a review and analysis. J. Volcanol. Geotherm. Res. 257, 135–158. https://doi.org/10.1016/j.jvolgeores.2013.02.014.

Mastin, L.G., Guffanti, M., Servranckx, R., Webley, P., Barsotti, S., Dean, K., et al., 2009. A multidisciplinary effort to assign realistic source parameters to models of volcanic ash-cloud transport and dispersion during eruptions. J. Volcanol. Geotherm. Res. 186 (1–2), 10–21. https://doi.org/10.1016/j.jvolgeores.2009.01.008.

McPhie, J., Walker, G.P.L., Christiansen, R.L., 1990. Phreatomagmatic and phreatic fall and surge deposits from explosions at Kilauea volcano, Hawaii, 1790 AD: Keanakakoi Ash Member. Bull. Volcanol. 52, 334–354. https://doi.org/10.1007/bf00302047.

Melnik, O.E., 2000. Dynamics of two-phase conduit flow of high-viscosity gas-saturated magma: large variations of sustained explosive eruption intensity. Bull. Volcanol. 62, 153–170. https://doi.org/10.1007/s004450000072.

Melnik, O., Sparks, R.S.J., 2002. Modelling of conduit flow dynamics during explosive activity at Soufrière Hills Volcano, Montserrat. In: Druitt, T., Kokelaar, B. (Eds.), The Eruption of Soufrière Hills Volcano, Montserrat, from 1995 to 1999. Geological Society, London, Memoirs vol. 21, pp. 307–317. https://doi.org/10.1144/GSL.MEM.2002.21.01.14.

Melnik, O., Sparks, R.S.J., 2005. Controls on conduit magma flow dynamics during lava dome building eruptions. J. Geophys. Res. 110, B02209. https://doi.org/10.1029/2004JB003183.

Mercalli, G., 1907. Vulcani attivi della Terra. Ulrico Hoepli.

Moitra, P., Gonnermann, H.M., Houghton, B.F., Tiwary, C.S., 2018. Fragmentation and Plinian eruption of crystallizing basaltic magma. Earth Planet. Sci. Lett. 500, 97–104. https://doi.org/10.1016/j.epsl.2018.08.003.

Nye, C., Keith, T., Eichelberger, J., Miller, T., McNutt, S., Moran, S., et al., 2002. The 1999 eruption of Shishaldin Volcano, Alaska: monitoring a distant eruption. Bull. Volcanol. 64, 507–519. https://doi.org/10.1007/s00445-002-0225-2.

Ort, M.H., Elson, M.D., Anderson, K.C., Duffield, W.A., Hooten, J.A., Champion, D.E., Waring, G., 2008a. Effects of scoria-cone eruptions upon nearby human communities. Geol. Soc. Am. Bull. 120, 476–486. https://doi.org/10.1130/B26061.1.

Ort, M.H., Elson, M.D., Anderson, K.C., Duffield, W.A., Samples, T.L., 2008b. Variable effects of cinder-cone eruptions on prehistoric agrarian human populations in the American southwest. J. Volcanol. Geotherm. Res. 176, 363–376. https://doi.org/10.1016/j.jvolgeores.2008.01.031.

Papale, P., 1999. Strain-induced magma fragmentation in explosive eruptions. Nature 397, 425–428. https://doi.org/10.1038/17109.

Papale, P., 2001. Dynamics of magma flow in volcanic conduits with variable fragmentation efficiency and nonequilibrium pumice degassing. J. Geophys. Res. 106, 11043–11065. https://doi.org/10.1029/2000JB900428.

Papale, P., Dobran, F., 1994. Magma flow along the volcanic conduit during the Plinian and pyroclastic flow phases of the May 18, 1980, Mount St. Helens eruption. J. Geophys. Res. 99, 4355–4373. https://doi.org/10.1029/93jb02972.

Parfitt, E.A., 2004. A discussion of the mechanisms of explosive basaltic eruptions. J. Volcanol. Geotherm. Res. 134, 77–107. https://doi.org/10.1016/j.jvolgeores.2004.01.002.

Parfitt, L., Wilson, L., 2008. Fundamentals of Physical Volcanology. John Wiley & Sons.

Petrelli, M., El Omari, K., Spina, L., Le Guer, Y., La Spina, G., Perugini, D., 2018. Timescales of water accumulation in magmas and implications for short warning times of explosive eruptions. Nat. Commun. 9, 770. https://doi.org/10.1038/s41467-018-02987-6.

Pietruszka, A.J., Garcia, M.O., 1999. The size and shape of Kilauea Volcano's summit magma storage reservoir: a geochemical probe. Earth Planet. Sci. Lett. 167 (3–4), 311–320. https://doi.org/10.1016/S0012-821X(99)00036-9.

Pioli, L., Erlund, E., Johnson, E., Cashman, K., Wallace, P., Rosi, M., Granados, H.D., 2008. Explosive dynamics of violent Strombolian eruptions: the eruption of Parícutin Volcano 1943-1952 (Mexico). Earth Planet. Sci. Lett. 271, 359–368. https://doi.org/10.1016/j.epsl.2008.04.026.

Polacci, M., Corsaro, R.A., Andronico, D., 2006. Coupled textural and compositional characterization of basaltic scoria: Insights into the transition from Strombolian to fire fountain activity at Mount Etna, Italy. Geology 34, 201–204. https://doi.org/10.1130/g22318.1.

Polacci, M., Baker, D.R., Mancini, L., Favretto, S., Hill, R.J., 2009. Vesiculation in magmas from Stromboli and implications for normal Strombolian activity and paroxysmal explosions in basaltic systems. J. Geophys. Res. Solid Earth 114 (B1). https://doi.org/10.1029/2008JB005672.

Polacci, M., Arzilli, F., La Spina, G., Le Gall, N., Cai, B., Hartley, M.E., et al., 2018. Crystallisation in basaltic magmas revealed via in situ 4D synchrotron X-ray microtomography. Sci. Rep. 8, 8377. https://doi.org/10.1038/s41598-018-26644-6.

Pompilio, M., Bertagnini, A., Carlo, P., Roberto, A., 2017. Magma dynamics within a basaltic conduit revealed by textural and compositional features of erupted ash: the December 2015 Mt. Etna paroxysms. Sci. Rep. 7, 4805. https://doi.org/10.1038/s41598-017-05065-x.

Richter, D.H., Eaton, J., Murata, K., Ault, W., Krivoy, H., 1970. Chronological narrative of the 1959-60 eruption of Kilauea volcano, Hawaii. US Geol. Surv. Prof. Pap. 73.

Romenski, E., Drikakis, D., Toro, E., 2010. Conservative models and numerical methods for compressible two-phase flow. J. Sci. Comput. 42, 68–95. https://doi.org/10.1007/s10915-009-9316-y.

Rosi, M., Principe, C., Vecci, R., 1993. The 1631 Vesuvius eruption. A reconstruction based on historical and stratigraphical data. J. Volcanol. Geotherm. Res. 58 (1–4), 151–182. https://doi.org/10.1016/0377-0273(93)90106-2.

Rosi, M., Bertagnini, A., Harris, A., Pioli, L., Pistolesi, M., Ripepe, M., 2006. A case history of paroxysmal explosion at Stromboli: timing and dynamics of the April 5, 2003 event. Earth Planet. Sci. Lett. 243 (3–4), 594–606. https://doi.org/10.1016/j.epsl.2006.01.035.

Rutherford, M.J., Papale, P., 2009. Origin of basalt fire-fountain eruptions on Earth versus the Moon. Geology 37 (3), 219–222. https://doi.org/10.1130/G25402A.1.

Schauroth, J., Wadsworth, F.B., Kennedy, B., von Aulock, F.W., Lavallée, Y., Damby, D.E., et al., 2016. Conduit margin heating and deformation during the AD 1886 basaltic Plinian eruption at Tarawera volcano, New Zealand. Bull. Volcanol. 78, 12. https://doi.org/10.1007/s00445-016-1006-7.

Scollo, S., Del Carlo, P., Coltelli, M., 2007. Tephra fallout of 2001 Etna flank eruption: analysis of the deposit and plume dispersion. J. Volcanol. Geotherm. Res. 160, 147–164. https://doi.org/10.1016/j.jvolgeores.2006.09.007.

Sigmundsson, F., Einarsson, P., Bilham, R., 1992. Magma chamber deflation recorded by the Global Positioning System: the Hekla 1991 eruption. Geophys. Res. Lett. 19 (14), 1483–1486. https://doi.org/10.1029/92GL01636.

Smith, R.L., 1979. Ash-Flow Magmatism. Ash-flow Tuffs: Geological Society of America Special Paper. vol. 180 pp. 5–27.

Smith, R.L., Shaw, H.R., 1973. Volcanic rocks as geologic guides to geothermal exploration and evaluation. Age, composition and volume. EOS Trans. Am. Geophys. Union 54 (11).

Smith, R.L., Shaw, H.R., 1978. Igneous-related geothermal systems. Assessment of Geothermal Resources of the United States, pp. 12–17.

Sparks, R.S.J., 1978. The dynamics of bubble formation and growth in magmas: a review and analysis. J. Volcanol. Geotherm. Res. 3, 1–37. https://doi.org/10.1016/0377-0273(78)90002-1.

Tait, S., Jaupart, C., Vergniolle, S., 1989. Pressure, gas content and eruption periodicity of a shallow, crystallising magma chamber. Earth Planet. Sci. Lett. 92 (1), 107–123. https://doi.org/10.1016/0012-821X(89)90025-3.

Valentine, G.A., 1998. Eruption column physics. In: Freundt, A., Rosi, M. (Eds.), From Magma to Tephra. Elsevier, Amsterdam, pp. 91–138.

Valentine, G.A., 2012. Shallow plumbing systems for small-volume basaltic volcanoes, 2: evidence from crustal xenoliths at scoria cones and maars. J. Volcanol. Geotherm. Res. 223, 47–63. https://doi.org/10.1016/j.jvolgeores.2012.01.012.

Valentine, G.A., Gregg, T., 2008. Continental basaltic volcanoes-processes and problems. J. Volcanol. Geotherm. Res. 177, 857–873. https://doi.org/10.1016/j.jvolgeores.2008.01.050.

Vergniolle, S., Jaupart, C., 1986. Separated two-phase flow and basaltic eruptions. J. Geophys. Res. Solid Earth (1978–2012) 91, 12842–12860. https://doi.org/10.1029/jb091ib12p12842.

Walker, G.P.L., 1973. Explosive volcanic eruptions—a new classification scheme. Geol. Rundsch. 62 (2), 431–446. https://doi.org/10.1007/BF01840108.

Walker, G.P.L., Self, S., Wilson, L., 1984. Tarawera 1886, New Zealand—a basaltic plinian fissure eruption. J. Volcanol. Geotherm. Res. 21, 61–78. https://doi.org/10.1016/0377-0273(84)90016-7.

Weisbach, J.L., 1845. Lehrbuch der Ingenieur- und Maschinen-Mechanik. Vieweg und Sohn, Braunschweig.

Williams, S.N., 1983. Plinian airfall deposits of basaltic composition. Geology 11, 211–214. https://doi.org/10.1130/0091-7613(1983)11<211:padobc>2.0.co;2.

Wilson, L., Head, J.W., 1981. Ascent and eruption of basaltic magma on the Earth and Moon. J. Geophys. Res. Solid Earth (1978–2012) 86, 2971–3001. https://doi.org/10.1029/jb086ib04p02971.

Wilson, L., Walker, G.P.L., 1987. Explosive volcanic eruptions-VI. Ejecta dispersal in plinian eruptions: the control of eruption conditions and atmospheric properties. Geophys. J. Int. 89 (2), 657–679. https://doi.org/10.1111/j.1365-246X.1987.tb05186.x.

Wilson, L., Sparks, R.S.J., Walker, G.P.L., 1980. Explosive volcanic eruptions IV. The control of magma properties and conduit geometry on eruption column behavior. Geophys. J. R. Astron. Soc. 63 (1), 117–148. https://doi.org/10.1111/j.1365-246X.1980.tb02613.x.

Woods, A.W., Koyaguchi, T., 1994. Transitions between explosive and effusive eruptions of silicic magmas. Nature 370, 641–644. https://doi.org/10.1038/370641a0.
Yoshida, S., Koyaguchi, T., 1999. A new regime of volcanic eruption due to the relative motion between liquid and gas. J. Volcanol. Geotherm. Res. 89, 303–315. https://doi.org/10.1016/S0377-0273(99)00005-0.
Zhang, Y., 1999. A criterion for the fragmentation of bubbly magma based on brittle failure theory. Nature 402, 648–650. https://doi.org/10.1038/45210.